A multiscale method coupling network and continuum models in porous media II – single and two phase flow

Jay Chu[*]   Björn Engquist[†]   Maša Prodanović[‡]   Richard Tsai[§]

Abstract

We present a numerical multiscale method for coupling a conservation law for mass at the continuum scale with a discrete network model that describes the pore scale flow in a porous medium. Our previously developed single-phase flow algorithm is extended to two-phase flow, for the situations in which the saturation profile go through a sharp transition from fully saturated to almost unsaturated states. Our coupling method for the pressure equation uses local simulations on small sampled network domains at the pore scale to evaluate the continuum equation and thus solve for the pressure in the domain. We present numerical results for single-phase flows with nonlinear flux-pressure dependence, as well as two-phase flow.

1   Introduction

In this paper, we extend the multiscale model [14] to compute pressure and saturation of two-phase flow in porous media. We also consider single-phase flow with nonlocal connectivity. The algorithm has the form of the heterogeneous multiscale method (HMM) [17], and couples a network model on the microscale with continuum scale over the same physical domain.

Modeling transport in the subsurface is extremely difficult. Nonlinearity and heterogeneity of small (pore) scale processes dictate the large scale flow behavior. At the pore scale, direct flow simulation in a detailed medium geometry assuming Stokes flow

---

[*]Department of Mathematics, The University of Texas at Austin, Austin, TX 78712-0257 (cc-chu@math.utexas.edu).

[†]Department of Mathematics and ICES, The University of Texas at Austin, Austin, TX 78712-0257(engquist@math.utexas.edu).

[‡]Department of Petroleum and Geosystems Engineering and CPGE, The University of Texas at Austin, Austin, TX 78712-0257(masha@ices.utexas.edu).

[§]Department of Mathematics and ICES, The University of Texas at Austin, Austin, TX 78712-0257(ytsai@math.utexas.edu).

is extremely costly. Network models [31, 6, 35] are a form of (semi)-upscaling where the complicated original geometry is mapped onto a representative network of idealized pores, throats, and cracks. The fluid displacements is then modeled as discrete events in the pore-throat network. At even larger scales, one usually constructs Darcy's law continuum models in which individual grid blocks contain sufficiently many pores such that the system within each grid block evolves smoothly with time. The specific micro structure of the pore space frequently plays a critical role in determining macroscopic flow properties, and often cannot be ignored. Continuum models accounting for two scales – the so-called dual porosity models [1, 2, 28]– have been constructed, and some efforts have also been made to build hybrid models [4, 39]. Balhoff et al. [4] focused on a scenario in which a pore network domain is connected to a continuum Darcy model for solving single-phase fluid flow. The network domain and continuum domain were physically disjoint except for a shared interface where information from the domains is exchanged. Another example is given in [3] where a mortar method is adapted to include pore scale models. The computational complexity of this technique was improved in [5].

We recently proposed a multiscale numerical method [14] based on the heterogeneous multiscale method (HMM) that couples network models and continuum equations for single-phase flow in porous media over larger length scales. The HMM [17], introduced by E and Engquist, is a general framework for designing multiscale methods. HMM starts with an incomplete macroscopic model for macro variables on the macrogrid covering the full domain. The missing quantities and data in the macroscopic model are obtained by solving an accurate microscale model locally over small domains. In Figure 1, we see an illustration of the how the proposed coupling is done. The continuum two-phase models in this paper are conservation laws written formally in two PDEs, one for the pressure and the other for the saturation of the fluids. The macroscopic PDEs are discretized over a grid using a finite volume method. The fluxes of the macroscopic variables through the cell that is outlined by the dashed rectangle are computed by network simulations over the four small domains. The network simulations over the small domains require boundary conditions that are determined by the values of the macroscopic variables. Typically, Dirichlet boundary conditions are imposed on the boundaries of each small domain. In such cases, one may simply interpolate the macroscopic variables to obtain the boundary data for the small network domains.

Our algorithm shares certain similarities with other upscaling approaches for both single phase flow [12, 10, 19, 32], and two phase flow [18, 11, 16]. We refer the reader to our previous paper [14] for an extensive comparison of conceptual approaches. Our algorithm couples a given pore scale network in 2D or 3D, structured or un-structured, to an effective conservation law on continuum scale that can be posed in 1D, 2D or 3D. The pore scale network properties may depend on effective quantities from the large scale.
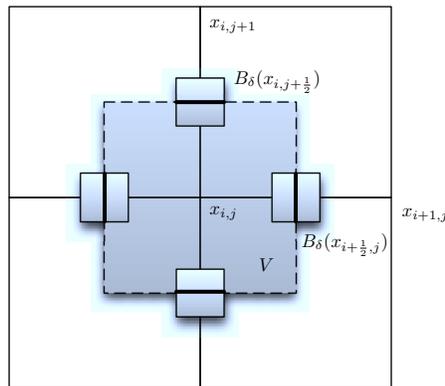
Figure 1: Schematic of 2D coupled model. The shaded cell with dashed boundary is a macro grid cell and the smaller shaded boxes on the four sides of the center box are local network domains.

2 Steady state single-phase flow

In this section, we present and analyze our original multiscale coupling algorithm. We will first describe our algorithm under the simplified assumption that the effective flow through the underlying two or three dimensional networks is essentially one dimensional and can be approximated by the effective continuum equations posed in one dimension. The results are generalized to higher dimensions and two-phase flow in Chapter 3.

2.1 Network Models

Generally speaking, predictions of macroscopic two-phase flow in a porous medium can be achieved by averaging of Navier-Stokes equations on the pore level assuming appropriate boundary conditions (this is how Darcy's equation can be derived [38]). However, obtaining a closed system of averaged equations requires the introduction of constitutive relationships between the different parameters, such as capillary pressure-saturation and relative permeability-saturation. These relationships can be obtained (or approximated) from pore scale simulations using direct simulation methods (lattice-Boltzmann method, smoothed particle hydrodynamics or a level set method, all of which work in exact porous medium geometry) or network models. Network flow modeling, pioneered by Fatt [22, 23, 24], retains the interconnectivity or the pathways in the original porous medium, as well as a set of micro-scale properties such as sizes of the pores (openings) and throats (tight cross-sections). The cross-sectional geometry shapes are, however, simplified which enables faster flow simulation. In contrast with averaging/homogenization approaches, network models stress capillary forces and their control of flow through the connected network of pores (openings, pore bodies, sites) and throats (narrow channels, necks, bonds). Reviews on network flow models by Celia
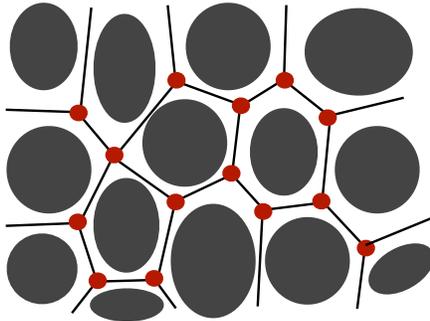
Figure 2: An example of the relation between a block of grains and a network model. In the network model, the grains are neglected, the pores are represented by balls (nodes) and the throats are represented by cylindrical tubes (segments).

et al. [9] and Blunt et al. [6, 7] have more details on the models and their historical development. Example network flow studies include relationship among saturation, capillary pressure and interfacial area [31], permeability prediction [8, 30], imbibition and drainage curves [26], phase distributions, relative permeability [30, 36, 37] and wettability [15].

In network models, pores are simply represented as nodes and throats as links (in simplest form they are cylindrical tubes). The nodes and tubes are usually depicted by vertices and edges respectively. Thus a network model has a topology of a graph. However, as each pore has a physical location, we shall refer a network that models a medium in a d dimensional domain as a d dimensional network. See Figure 2 for an illustration of a two dimensional network.

In Experiment 2, we test the scenario where the length scales of the network throats and the magnitudes of the conductance are not clearly separated – this is an idealized situation of e.g. a partially cemented natural fracture [29] or man-made structure (wellbore or a drain pipe) that connects two non-neighboring porous regions and represents a "highway" connection for fluid flow between them. Of course, we can also model situations where the high conductivity channel is connected to the formation along its length (and in essence do so, in 2D, in [14]), but this particular experiment (in addition to modeling a different situation) poses higher numerical stability issues.

For convenience, we number all nodes in the domain and collect them in the set I. Furthermore, we shall denote by $I^{(0)}$ the index set containing all the indices of the nodes lying in the interior of the network domain. Let I_i denote the set consisting of all node indices j that connect to the node i by a throat. Further, p_i denotes the microscopic pressure inside pore i and c_{ij} denotes the conductance of the throat which connects pore i and the pore j for each $j \in I_i$. The pressure flux from pore i to pore j is simply $c_{ij}(p_i - p_j)$. The law of mass conservation leads to

$$\sum_{j \in I_i} c_{ij}(p_i - p_j) = g_i, \tag{1}$$

4

where g_i is the sink or source in the pore i. In general, the conductance c_{ij} may be a nonlinear function,

$$c_{ij} := c(p_i, p_j), \qquad (2)$$

depending on the nearby pressure p_i and p_j. However, for particular cases such as Newtonian fluid in a cylindrical throat where gravity can be ignored, the conductance is given by a constant

$$c_{ij} = \frac{\pi r^4}{8\, l \mu},$$

where r is the radius and l the length of the throat, and μ is the viscosity of the fluid. System (1) should be coupled with suitable boundary conditions on the boundary nodes. The boundary conditions are typically Dirichlet, periodic or Neumann conditions.

In this section, we assume a three dimensional network, and we impose Dirichlet boundary conditions on two opposite faces (the left and the right faces) of the cubic volume and periodic boundary condition (or no flow condition) on the remaining parts of the boundary. Periodic boundary conditions can be used in regular lattice networks, as well as in irregular networks from periodic model sphere packings.

Let I_{x_0} the index set consisting the indices of the nodes that are connected by throats that cut through the plane $x = x_0$. Then the flux through this plane is computed by summing up the fluxes through all the throats that cross this plane:

$$f = \sum_{i \in I_{x_0}} \sum_{j \in I_i} c_{ij}(p_i - p_j). \qquad (3)$$

2.2 Macroscopic Model

Consider a network model over the domain $[x_L, x_R] \times [y_1, y_2] \times [z_1, z_2]$, with Dirichlet on the boundaries at x_L and x_R, and periodic boundary condition (or no flow Neumann) on the other 4 faces. Let $B_\delta(x)$ be the subdomain $[x - \delta/2, x + \delta/2] \times [y_1, y_2] \times [z_1, z_2]$ and $\Sigma(x; \delta)$ be the boundary surface of $B_\delta(x)$. By integrating (26) over $B_\delta(x)$ and applying the boundary conditions, we have

$$\int_{B_\delta} G\, dv = \int_{B_\delta} \nabla \cdot \mathbf{v}\, dv = \oint_\Sigma \mathbf{v} \cdot \mathbf{n}\, ds = F_{\Sigma_R} - F_{\Sigma_L}, \qquad (4)$$

where F_{Σ_R} and F_{Σ_L} are the fluxes through boundaries at $x + \delta/2$ and $x - \delta/2$ respectively. Dividing δ on the both sides of (4) and taking the limit as δ to 0 lead to

$$\frac{d}{dx} F = \lim_{\delta \to 0} \frac{1}{\delta} \int_{B_\delta(x)} G dv =: Q(x), \qquad x \in (x_L, x_R). \qquad (5)$$

Hence we obtain a one dimensional macroscopic equation over $[x_L, x_R]$ with the macroscopic pressure P being the unknown which can be viewed as an average pressure of small scale pressure p on the cross section $\Sigma(x; 0)$. We assume the flux F is a function of pressure P, pressure gradient P_x and location x. We shall evaluate F from simulations using the network models.

5

Let N be the number of partitions of $[x_L, x_R]$ and $\Delta x = (x_R - x_L)/N$, $x_l = x_L + l\Delta x$ for $l = 0, 1, ..., N$, . Let P_l be the approximation of $P(x_l)$ and $F_{l-\frac{1}{2}}$ be the approximation of the flux F at $x_{l-\frac{1}{2}} = (x_l + x_{l-1})/2 = x_L + (l - \frac{1}{2})\Delta x$. The main goal of our multiscale method is to find $P_0, P_1, P_2, ..., P_{N-1}, P_N$ such that $P_0 = P_L$, $P_N = P_R$ and

$$F_{l+\frac{1}{2}} - F_{l-\frac{1}{2}} = \int_{x_{l-\frac{1}{2}}}^{x_{l+\frac{1}{2}}} Q dx =: Q_i \Delta x \quad \text{for } l = 1, 2, ..., N - 1. \tag{6}$$

In the next subsection, we describe how to evaluate the macroscopic fluxes and how to map the macroscopic fluxes to the values of the macroscopic pressures.

2.3 The basic coupling algorithm

The macroscopic flux $F_{l-\frac{1}{2}}$ is determined by the network model as follows. For each grid node x_l, we choose a representative subdomain $B_\delta(x_{l-\frac{1}{2}})$. We call the corresponding portion of our network over this subdomain the local network centered at $x_{l-\frac{1}{2}}$. The Dirichlet boundary conditions for the subdomain $B_\delta(x_{l-\frac{1}{2}})$ at $x_{l-\frac{1}{2}} \pm \delta/2$ are defined as the values of the macroscopic at the corresponding locations. At the discretization level, they are approximated by linear interpolation of P_l and P_{l-1} on $[x_{l-1}, x_l]$ to define an approximation of the pressure P at $x_{l-\frac{1}{2}} \pm \delta/2$. Thus, the flux through the local network is a function depending on two macroscopic pressure values and the center of the subdomain

$$\hat{f}_{l-\frac{1}{2}} = f(x_{l-\frac{1}{2}}, P_{l-1}, P_l),$$

where f is the function defined by (3) in Section 2.1. More precisely, the Dirichlet boundary conditions at $x_{l-\frac{1}{2}} \pm \frac{\delta}{2}$ are $P_{l-\frac{1}{2}, L}$ and $P_{l-\frac{1}{2}, R}$ defined by $P_{l-\frac{1}{2}} = (P_{l-1} + P_l)/2$, and

$$P_{l-\frac{1}{2}, L} = P_{l-\frac{1}{2}} - D^+ P_{l-1}(\delta/2), \quad P_{l-\frac{1}{2}, R} = P_{l-\frac{1}{2}} + D^+ P_{l-1}(\delta/2),$$

where $D^+ P_{l-1} = (P_l - P_{l-1})/\Delta x$ is the standard divided centered differencing on P_{l-1}.

The macroscopic flux $F_{l-\frac{1}{2}}$ is defined as the flux, denoted by $\hat{f}_{l-\frac{1}{2}}$, through the corresponding local network:

$$F_{l-\frac{1}{2}}(P_{l-1}, P_l) = \hat{f}_{l-\frac{1}{2}}.$$

The source term $\int_{x_{l-\frac{1}{2}}}^{x_{l+\frac{1}{2}}} Q \, dx = \int_B S dv$ is obtained by summing all source term s_i in each pores inside subdomain B. In particular, $Q_i \Delta x = \int_{x_{l-\frac{1}{2}}}^{x_{l+\frac{1}{2}}} G dx = 0$ if we assume $g_i = 0$ in the network model.

Figure 3 shows a schematic diagram of the proposed coupling. The dashed boxes show there correspond to the representative local networks, which can be two or three dimensions. Under this setting, *the flux F can be obtained for any given pressures P_{l-1} and P_l, but the explicit expression is unknown, when the underlying network model is*
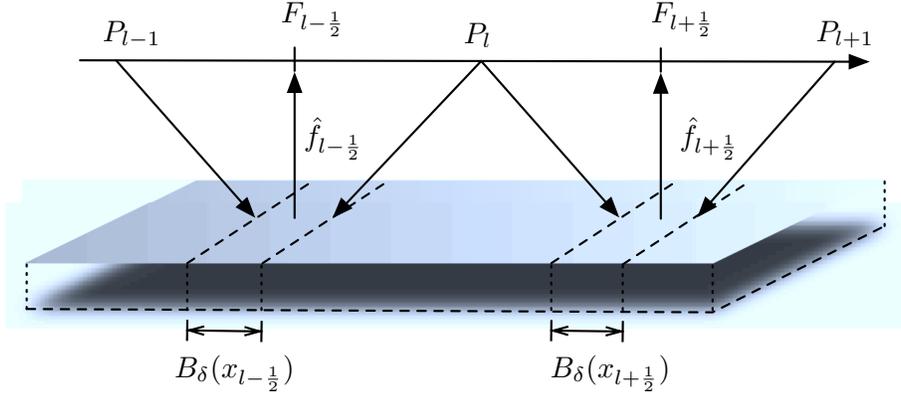
Figure 3: Continuous (macro) scale is discretized using points $x_l, l = 0, .., N$. Macro flux $F_{l-\frac{1}{2}}$ is updated using micro scale simulation (network model) on a representative region within the segment $[x_{l-1}, x_l]$ (local network domain). At the same time, the boundary conditions (in this sketch, pressure boundary conditions) required for the micro-scale model come from the macro-scale information (pressure) at end points $[x_{l-1}, x_l]$.

nonlinear. The formal algebraic equations (6) for the macroscopic pressure P_l may be nontrivial to solve as the relation between $F_{l-\frac{1}{2}}$, P_{l-1} and P_l are not available explicitly. In particular, the Newton's method is not applicable and thus an alternate root finding scheme is required. We propose a quasi-Newton-like scheme in next section.

2.3.1 Recovering the pressure from macroscopic flux values

We now describe our proposed method for recovering the macroscopic pressure values. In the following discussion, we first assume that there is no source term in the system. As one can see from the above discussion, the difficulty to be overcome here is that no convenient analytical relation between the macroscopic flux F and the pressure P is available (or rather assumed). Our strategy is resort to Taylor expansions, using the fact that the flux should be zero when there is no pressure gradient; i.e.

$$F(x, P, P_x) = f(x, P, P_x) = 0, \quad \text{whenever } P_x = 0,$$

and thus

$$F(x, P, P_x) = F_{P_x}(x, P, \xi)P_x, \tag{7}$$

where F_{P_x} refers to the partial derivative of F with respect to third variable and ξ is an intermediate value, which depends on P and x, between 0 and P_x.

At the discrete level, we want to solve the following equations for P_l:

$$F(x_{l+\frac{1}{2}}, P_{l+\frac{1}{2}}, D^+ P_l) = \hat{f}_{l+\frac{1}{2}}(P_l, P_{l+1}). \tag{8}$$

$$D^- F(x_{l+\frac{1}{2}}, P_{l+\frac{1}{2}}, D^+ P_l) = Q_l \Delta x, \ l = 1, 2, \cdots, N-1, \tag{9}$$

with the boundary condition $P_0 = P_L, P_N = P_R$. See Figure 3 for a diagram. Therefore, we use

$$F(x_{l+\frac{1}{2}}, P_{l+\frac{1}{2}}, D^+ P_l) = F_{P_x}(x_{l+\frac{1}{2}}, P_{l+\frac{1}{2}}, \xi) \approx \hat{f}_{l+\frac{1}{2}}(P_l, P_{l+1})/D^+ P_l =: -K(P_l, P_{l+1}). \tag{10}$$

We propose to solve the above coupled equations by iterations:

$$-D^- \left(K(P_l^{(n)}, P_{l+1}^{(n)}) D^+ P_l^{(n+1)} \right) = Q_l \Delta x. \tag{11}$$

This iterative scheme can be explicitly written as

$$\mathbf{P}^{(n+1)} = (\frac{1}{\Delta x^2} \mathbf{K}^{(n)})^{-1} \mathbf{h}^{(n)} = \mathbf{P}^{(n)} - (\frac{1}{\Delta x^2} \mathbf{K}^{(n)})^{-1} \mathbf{G}(\mathbf{P}^{(n)}), \tag{12}$$

where

$$K_{l-\frac{1}{2}}^{(n)} = F_{l-\frac{1}{2}}^{(n)} \cdot \frac{\delta}{(P_{l-\frac{1}{2}, L}^{(n)} - P_{l-\frac{1}{2}, R}^{(n)})} = -\frac{F_{l-\frac{1}{2}}^{(n)}}{D^+ P_{l-1}^{(n)}}, \tag{13}$$

$$\mathbf{K}^{(n)} = \begin{pmatrix} K_{\frac{1}{2}}^{(n)} + K_{\frac{3}{2}}^{(n)} & -K_{\frac{3}{2}}^{(n)} & 0 & \cdots & 0 \\ -K_{\frac{3}{2}}^{(n)} & K_{\frac{3}{2}}^{(n)} + K_{\frac{5}{2}}^{(n)} & -K_{\frac{5}{2}}^{(n)} & \ddots & \vdots \\ 0 & -K_{\frac{5}{2}}^{(n)} & \ddots & \ddots & 0 \\ \vdots & \ddots & \ddots & \ddots & -K_{N-\frac{3}{2}}^{(n)} \\ 0 & \cdots & 0 & -K_{N-\frac{3}{2}}^{(n)} & K_{N-\frac{3}{2}}^{(n)} + K_{N-\frac{1}{2}}^{(n)} \end{pmatrix}, \tag{14}$$

$$\mathbf{h}^{(n)} = [Q_1 + K_{1-\frac{1}{2}}^{(n)} P_L/\Delta x^2, Q_2, ..., Q_{N-2}, Q_{N-1} + K_{N-\frac{1}{2}}^{(n)} P_R/\Delta x^2]^T, \tag{15}$$

and

$$\mathbf{G}(\mathbf{P}) = \left[D^+ F_{1-\frac{1}{2}} - Q_1, D^+ F_{2-\frac{1}{2}} - Q_2, ..., D^+ F_{N-1-\frac{1}{2}} - Q_{N-1} \right]^T. \tag{16}$$

We refer the readers to [14] for more detailed discussion about this iterative scheme and its convergence. The treatment for the cases involving non-zero source terms is also presented in [14].

3   Two-Phase Flow

In this section, we generalize the coupling algorithm described in the previous section to couple multi-dimensional continuous equations with a dynamic two-phase flow network models. The dynamic network model follows the work of Joekar-Niasar, Hassanizadeh and Dahle [27]. For completeness, we summarize their algorithm in the following section.

3.1 Two-Phase Dynamic Pore-Network Modeling

In the model of [27], each pore is filled with one or two fluids (wetting and non-wetting), and each fluid has its own pressure, denoted by p^w and p^n respectively. The local capillary pressure p_i^c for pore body i is defined as the difference of non-wetting and wetting pressure. The capillary pressure is assumed to be determined by local saturation s^w in the pore body i only. That is,

$$p_i^c = p_i^n - p_i^w = p_i^c(s^w). \qquad (17)$$

A flux f_{ij}^α for phase α fluid in throat ij is simply given by

$$f_{ij}^\alpha = c_{ij}^\alpha(p_i^\alpha - p_j^\alpha), \quad \alpha = w, n \qquad (18)$$

where c_{ij}^α is the conductance of the throat for phase α fluid. Since the flow is incompressible, the mass conservation law implies the total mass is conserved:

$$\sum_{j \in I_i} f_{ij}^w + f_{ij}^n = \sum_{j \in I_i} c_{ij}^w(p_i^w - p_j^w) + c_{ij}^n(p_i^n - p_j^n) = g_i, \qquad (19)$$

where g_i describes either the sink or the source in pore i. For simplicity, we assume $g_i = 0$ for all pores. To reduce the numbers of unknowns in (17) and (19), the pressure equation (19) is reformulated in terms of total pressure $\bar{p}_i = s_i^w p_i^w + s_i^n p_i^n$:

$$\sum_{j \in I_i}(c_{ij}^w + c_{ij}^n)(\bar{p}_i - \bar{p}_j) = -\sum_{j \in I_i}[(c_{ij}^n s_i^w - c_{ij}^w(1 - s_i^w)) + (c_{ij}^w(1 - s_j^w) - c_{ij}^n s_j^w)p_j^c]. \quad (20)$$

Notice that for given conductance c^n and c^w, only boundary condition $\bar{p}$ and saturation s are involved to solve (20) since p^c depends on s also. Once $\bar{p}$ is solved, $p^w = \bar{p} - s^n p^c$, $p^n = \bar{p} + s^w p^c$ and fluxes f_{ij}^n and f_{ij}^w in each throats can be calculated.

For saturation, a volume balance for each fluid gives

$$V_i \frac{\Delta s_i^\alpha}{\Delta t} = -\sum_{j \in I_i} f_{ij}^\alpha, \qquad (21)$$

where V_i is the volume of the pore i. Equations (17), (19) and (21) form a complete set of governing equations for two-phase dynamic pore-network modeling. Typically the boundary conditions of pressure and saturation are Dirichlet on one pair of opposite faces (or sides for 2D), and periodic on the rest of faces (or sides). In our later simulation, the local network model is under this setting and the Dirichlet boundary conditions are determined by near by coarse scale pressure and saturation.

In the following, we summarize how to evolve the saturation, as proposed in [27], using equations (17), (19), and (21). We start with the given initial saturation data and boundary conditions are given for both pressure and saturation.

Step 1. Compute the local capillary pressure. The local capillary pressure p_i^c is a function depending on the wetting phase saturation s_i^w and the interfacial tension

σ^{nw}. Detail of the function is derived from the shape of the pore body. An example is presented In Experiment 3.

Step 2. Determine if a throat is invaded by the non-wetting phase. A throat is invaded when the capillary pressure in a neighboring pore body is larger than the entry capillary pressure (a critical value) of the throat α_{ij}. In this case, we assign the capillary pressure in the throat p_{ij}^c to be equal to the capillary pressure of the upstream pore body. That is, if $\alpha_{ij} < p_i^c$ (or $\alpha_{ij} < p_i^c$), then the throat ij is invaded and $p_{ij}^c = p_i^c$ (or $p_{ij}^c = p_j^c$).

Step 3. Calculate the conductances of throats. There are two cases during the simulation:

Case 1: The throat is not invaded by the non-wetting phase. Then the conductances are obtained by

$$c_{ij}^w = \frac{\pi}{8\mu^w l_{ij}} \left(\sqrt{\frac{4}{\pi}} \, r_{ij} \right)^4 \quad \text{and} \quad c_{ij}^n = 0,$$

where r_{ij} and l_{ij} are the inscribed radius and length of the throat ij respectively, and μ^w is the viscosity of the wetting phase.

Case 2: The throat is invaded by the non-wetting phase. Then the conductances of each phases are given by

$$c_{ij}^w = \frac{4-\pi}{\beta\mu^w l_{ij}}(r_{ij}^c)^4 \quad \text{and} \quad c_{ij}^n = \frac{\pi}{8\mu^n l_{ij}}(r_{ij}^{eff})^4,$$

where μ^n is the viscosity of the non-wetting phase and

$$r_{ij}^c = \frac{\sigma^{nw}}{p_{ij}^c}, \quad \text{and} \quad r_{ij}^{eff} = \frac{1}{2} \left(\sqrt{\frac{r_{ij}^2 - (4-\pi)(r_{ij}^c)^2}{\pi}} + r_{ij} \right).$$

Here β is a resistance factor that depends on the geometry of the throats (See [40]).

Step 4. Solve pressure equations (20) with the given Dirichlet boundary conditions to get fluxes f_{ij}^n and f_{ij}^w in each throats.

Step 5. Update saturation s_i^w. Once flux f_{ij}^w is obtained, saturation of next time step can be updated by discretizing equation (21) explicitly, for example, Euler scheme. However, the explicit saturation update scheme may be unstable [34]. Therefore, Joekar-Niasar et. al. proposed a semi-implicit scheme to overcome this difficulty [27]. Their scheme uses total flux $f_{ij}^{tot} = f_{ij}^w + f_{ij}^n$ and total conductance $c_{ij}^{tot} = c_{ij}^w + c_{ij}^n$ as unknowns. The non-wetting flux f_{ij}^n is related to the total flux by a formula analogous to the fractional-flow equation:

$$f_{ij}^n = \frac{c_{ij}^n}{c_{ij}^{tot}} f_{ij}^{tot} + \frac{c_{ij}^n c_{ij}^w}{c_{ij}^{tot}}(p_i^c - p_j^c). \tag{22}$$

The key in their scheme is to approximate $p_i^c - p_j^c$ by derivatives with respect to s^w:

$$p_i^c - p_j^c = \frac{\partial p_{ij}^c}{\partial s_{ij}^w}(s_i^w - s_j^w). \tag{23}$$

Similar to p_{ij}^c, $\partial p_{ij}^c / \partial s_{ij}^w$ is calculated from the upstream pore body. By substituting (23) into (22), a semi-implicit discretization of (21) is given by

$$V_i \frac{(s_i^w)^{k+1} - (s_i^w)^k}{\Delta t} - \sum_{j \in I_i} \left(\frac{c_{ij}^n}{c_{ij}^{tot}} f_{ij}^{tot} + \frac{c_{ij}^n c_{ij}^w}{c_{ij}^{tot}} \frac{\partial p_{ij}^c}{\partial s_{ij}^w} \left((s_i^w)^{k+1} - (s_j^w)^{k+1} \right) \right) = 0. \quad (24)$$

After updating saturation, go back to Step 1 and repeat the process until the saturation is unchanged.

3.2 Two-phase flow continuum model

The two-phase flow cases that we consider involve a wetting and a non-wetting fluids. We use the saturation (volume fraction) S^w to denote the ratio between the volume of wetting fluid and the total volume of pore space. The saturation of non-wetting phase S^n is defined analogously. Obviously the saturations satisfies $S^w + S^n = 1$. Due to the curvature and surface tension of the interface of the two phases, the pressure in the non-wetting fluid P^n is higher than that in wetting fluid P^w; the pressure difference is determined by the capillary pressure $P^c = P^n - P^w$. The balance of volume for phase saturation result in the following evolution equations:

$$\phi \frac{\partial S^\alpha}{\partial t} + \nabla \cdot \mathbf{v}^\alpha = 0, \quad \alpha = w, n, \quad (25)$$

where ϕ is the porosity, the ratio of the volume of all the pores to the total volume, of the medium, and $\mathbf{v}^\alpha$ is the average velocity for phase α.

This model can be simplified by the introduction of the so-called global pressure P and the total fluid velocity $\mathbf{v} = \mathbf{v}^w + \mathbf{v}^n$; see [13]. In the simplified model, the mass conservation equation is written as

$$\nabla \cdot \mathbf{v}(\mathbf{x}, P, \nabla P, S^w) = G(\mathbf{x}), \quad (26)$$

where G is a source or sink term. The saturation equations (25) are reduced to a single one involving the evolution of S^w:

$$\phi \frac{\partial S^w}{\partial t} + \nabla \cdot (f(S^w)\mathbf{v}) = 0, \quad (27)$$

where f is the fractional flow of wetting fluid. In classical models, the velocity is assumed to satisfy Darcy's law: $\mathbf{v} = -\kappa(\mathbf{x}, S^w)\nabla P$. The positive definite tensor function $\kappa(\mathbf{x}, S^w)$ may depend on saturation S^w. A common form of $\kappa(\mathbf{x}, S^w)$ is $\kappa(\mathbf{x}, S^w) = \lambda(S^w)\kappa$, where κ is the absolute permeability and $\lambda(S^w)$ is mobility. By Darcy's law, equation (26) becomes an elliptic partial differential equation:

$$-\nabla \cdot (\kappa(\mathbf{x}, S^w)\nabla P) = G(\mathbf{x}). \quad (28)$$

Equations (28) and (27) are called the pressure and saturation equations respectively. In our work, the coarse pressure is simply describe by global pressure P and we do not

covert P to single-phase pressure P^w or P^n. The flux are directly estimated from local network simulation without using fractional flow information. Therefore the details about formulas of global pressure P and the fractional flow f are omitted here and we refer interested readers to [13] for more information.

The capillary force is usually neglected in pressure and saturation equations, or is embedded as a factor in the mobility λ and fractional flow function f. In this paper, we assume the macroscopic model is given by equations (26) and (27), and the capillary pressure effect is captured through coupling local network model.

3.3   Coupling for Two-Phase Flow

In this section, we explain how to couple the network modeling described in the previous section with the following continuum conservation laws:

$$\nabla \cdot \mathbf{v}(\mathbf{x}, P, \nabla P, S^w) = 0, \tag{29}$$

$$\phi \frac{\partial S^w}{\partial t} + \nabla \cdot \mathbf{v}^w = 0. \tag{30}$$

Here S^w is the average saturation for wetting phase, P is the average pressure and ϕ is the porosity, and we assume the source term $G = 0$ for simplicity. Recall that $\mathbf{v}^w$ is the velocity for wetting phase and total velocity $\mathbf{v} = \mathbf{v}^w + \mathbf{v}^n$.

We adapt implicit pressure and explicit saturation (IMPES) approach: First we fix saturation S^w and solve (29) to get updated pressure P. Below we describe details of each step separately in two dimensional problems, but the method can be easily generalized to three-dimensional problems.

3.3.1   Solution of the pressure equation

We evaluate the flux for α phase fluid by $F^\alpha = \int_\Sigma \mathbf{v}^\alpha \cdot \mathbf{n} \, ds$ through suitable surfaces Σ for different profiles of P, and total flux is given by $F = F^w + F^n$. On the other hand, the macro-quantities (macroscopic pressure and saturation) determine the boundary conditions for the local network simulations and value of saturation that are used to evaluate the total flux. As in the single-phase case, the coupled system is solved by iteration, starting with the initial macroscopic data for the saturation, and some initial guess for the macroscopic pressure. Local network simulations are performed to evaluate the macroscopic fluxes. The macroscopic saturation and pressure are then updated.

We use a finite volume discretization to solve the PDEs (29) on a rectangular domain. Divide the domain into $N_1 \times N_2$ coarse blocks. On each coarse grid, we assign average pressure $P_{i,j}$ and saturation $S^w_{i,j}$. Let $\mathbf{x}_o$ be the center of a block, and V be the corresponding control volume. See Figure 1 for an illustration. Hence, (29) implies that

$$\oint_{\partial V} \mathbf{v} \cdot \mathbf{n} \, ds = 0 \tag{31}$$

Let F_N, F_S, F_W, and F_E denote the total fluxes through the four edges of V. Equation (31) implies

$$F_N + F_S + F_W + F_E = 0. \tag{32}$$

The total flux F across each side of V is evaluated by $\hat{f}$ coming from local network simulations on a $\delta \times \delta$ size sampling domain B_δ with boundary condition from given macroscopic pressure P and saturation in each pore from downscaling macro saturation S^w. We describe in detail the case of computing F_E below. The fluxes through the other edges of V can be easily computed analogously. We define

$$F_E(\mathbf{x}_{i+\frac{1}{2},j}) = \mathbf{v}_{i+\frac{1}{2},j} \cdot \mathbf{n}_x \, \Delta y = \hat{f}^{(x)}(P_{i,j}, P_{i+1,j}) \Delta y / \delta,$$

where $\hat{f}^{(x)}$ is the total flux through the local network over $B_\delta(\mathbf{x}_{i+\frac{1}{2},j})$ in x-direction. The dependence of $P_{i,j}$ and $P_{i+1,j}$ comes from the boundary condition interaction. More precisely, $\hat{f}^{(x)}$ is evaluated from a local network simulation according to Steps 1, 2, 3, 4 described in Section 3.1. The saturation s_i used in the local network is obtained from interpolating coarse saturation S^w. A particular downscaling method of coarse saturation S is presented in Section 3.3.2. Combining with boundary condition from interpolation of coarse pressure, total flux $f = f^w + f^n$ can be calculated by solving $\bar{p}$ in Step 4. Under this setting, the flux is a function of macroscopic pressure, and we look for macroscopic pressure $P_{i,j}$ such that the corresponding flux satisfies (32). For simplicity, we assume the upsaled conductance is isotropic. The boundary conditions for local network simulation is setup as Dirichlet boundary condition in x-direction and periodic boundary conditions in y-direction. The Dirichlet boundary condition is computed by linear interpolation using $P_{i,j}$ and $P_{i+1,j}$. For anisotropic upscaled conductance, we can apply more complicated boundary condition that is discussed in [14].

As in the one dimensional case, an explicit algebraic formula for the macroscopic flux F as a function of pressure and pressure gradient is not readily available. Moreover, due to capillary pressure inside the network, $\hat{f}^{(x)}$ can be nonzero even the boundary conditions are the same on both sides. However, from Taylor expansion, we have

$$\hat{f}^{(x)}(P_{i,j}, P_{i+1,j}) = \hat{f}^{(x)}(P_{i,j}, P_{i,j} + \Delta^+ P_{i,j}) = \hat{f}^{(x)}(P_{i,j}, P_{i,j}) + \partial_2 \hat{f}^{(x)}(P_{i,j}, \xi) \Delta^+ P_{i,j},$$

where $\Delta^+ P_{i,j} = P_{i+1,j} - P_{i,j}$, ∂_2 is the partial derivative operator with respect to second variable and ξ is an intermediate value of $P_{i,j}$ and $P_{i+1,j}$. In the macroscopic scale, $\hat{f}^{(x)}(P_{i,j}, P_{i,j})$ is usually small and can be neglected. Hence

$$\hat{f}^{(x)}(P_{i,j}, P_{i+1,j}) \simeq \partial_2 \hat{f}^{(x)}(P_{i,j}, \xi) \Delta^+ P_{i,j}.$$

On the other hand, the macro flux F_E defined in (3.3.1) can be written as

$$F_E := \hat{f}^{(x)}(P_{i,j}, P_{i+1,j}) \frac{\Delta y}{\delta} = (K_{i+\frac{1}{2},j} D_+^x P_{i,j}) \Delta y, \tag{33}$$

where $K_{i+\frac{1}{2},j}$ is given by

$$K_{i+\frac{1}{2},j} = \hat{f}^{(x)}(P_{i,j}, P_{i+1,j})/(\delta \, D_+^x P_{i,j}). \tag{34}$$

13
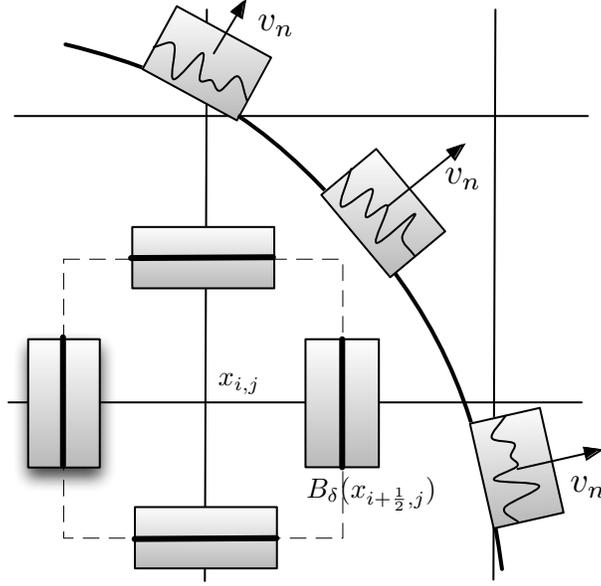
Figure 4: Microscale network simulations of the two-phase model are performed in the shaded boxes. The boxes B_δ at the edges of the macro cells are used in the pressure calculation and the boxes along the front determine the macroscale front velocity.

and $D_+^x P_{i,j}$ is the forward difference. A simple calculation can show that $K_{i+\frac{1}{2},j} \simeq \partial_2 \hat{f}^{(x)}(P_{i,j}, \xi)\Delta x/\delta$.

Now we are ready to describe our Macro-micro iterations. For a given macroscopic pressure $P_{i,j}^{(n)}$, we compute the coefficients $K_{i\pm\frac{1}{2},j}^{(n)}$ and $K_{i,j\pm\frac{1}{2}}^{(n)}$ as in (34). The updated macroscopic pressure $P_{i,j}^{(n+1)}$ is obtained by solving the sparse linear system

$$F_N^{(n)} + F_S^{(n)} + F_W^{(n)} + F_E^{(n)} = 0,$$

where

$$F_E^{(n)} = \left(K_{i+\frac{1}{2},j}^{(n)} D_+^x P_{i,j}^{(n+1)} \right) \Delta y,$$

$$F_N^{(n)} = \left(K_{i,j+\frac{1}{2}}^{(n)} D_+^y P_{i,j}^{(n+1)} \right) \Delta x.$$

Under certain assumptions, the iterations converge to a solution of (32). See [14] for more detail.

3.3.2 Evolution of the saturation

We consider a simplified but commonly occurring setting of multiphase flow in porous media for drainage process. In a drainage process, one injects a non-wetting fluid into

a bulk volume that is initially filled with a wetting fluid. The initial saturation is equal to 1 for all pores except ones on the injecting boundary. The boundary condition is simply $s = 1$ on the injecting side and $s = 0$ on the opposite side. In the evolution of saturation usually forms a sharp transition layer through which the saturation goes from 0 to 1. We refer this transition layer as a front.

In this setting, the macro saturation is simply characterize by a evolving curve $\Gamma(t)$ that represents the interface of a sharp transition from $S = 1$ to $S = S_0 \sim 0$. For a given front $\Gamma(t)$, we first downscale the macro saturation to pore scale saturation by: if a pore is ahead $\Gamma(t)$, then its saturation is 1; if a pore is behind $\Gamma(t)$, then its saturation is set to be its minimum saturation. Physically due to the shape of pore bodies, it is impossible to displace the wetting phase by non-wetting phase in each pore. Thus each pore body has a minimum saturation $s_{i,min}^w$. This minimum saturation depends on geometry of pore bodies. An example of defining the minimum saturation is given in Experiment 3. Similarly, a throat is invaded or not is determined by its location. If both end pores of the throat are behind $\Gamma(t)$, then the throat is marked as invaded. Otherwise, the throat is not invaded. The downscaled information is used in local network to calculate macroscopic pressures P as discussed in Section 3.3.1.

The evolution of $\Gamma(t)$ is approximated by advancing a certain number of points on marked points $\Gamma(t)$. At each time t_n, the speed of the marked point is evaluated from two-phase network simulations performed on a local network whose size is $\delta \times \delta$. The orientation of the local network coincides with the normal direction of $\Gamma(t)$ at the marked point. The marked point is at the center of the side of the sampling domain that is tangent to $\Gamma(t)$. Thus, we have a multiscale front propagation problem, see Figure 4 for an illustration. Similar approaches have been used to study combustion [21] as well as epitaxial crystal growth [20].

The initial and boundary conditions used in each local network placed over the front is set up as following. The initial values for the saturations are from downscaling macroscopic saturation as described above. Boundary conditions for the saturations: 0 and 1 in the two normal sides and periodic in the tangential sides. Boundary conditions for the pressure is Dirichelt boundary conditions in the two normal sides and periodic in the tangential sides. The Dirchlet boundary conditions for the microscopic pressures are obtained from interpolating the macroscopic pressures P at the grid. The local network simulation is performed for τ amount of time to obtain the change in saturation. The speed of the marked point is calculated by

$$\frac{\delta \cdot |\sum_i V_i(s_i^{new} - s_i^{old})|}{\tau \sum_i V_i},$$

where V_i, s_i^{old} and s_i^{new} are the volume, the initial saturation and saturation at τ of pore i respectively. In Figure 5, we present three snapshots of saturation in a local simulation used in Experiment 3. We evolve $\Gamma(t)$ with a time step size Δt bigger than τ by moving the marked points in the normal directions with distance equal to the product of their speed and Δt.

15
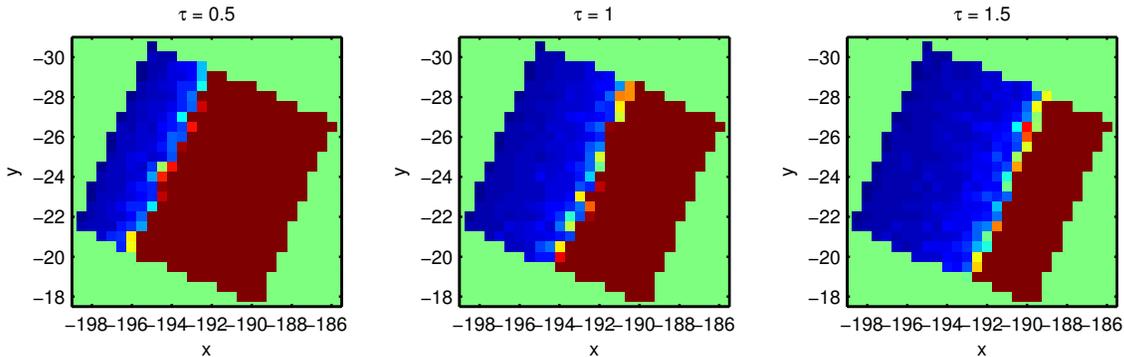
Figure 5: Snapshot of saturation of local network simulation at different time $\tau = 0.5, 1, 1.5$. Change of saturation in the local network is used to calculate speed of the front at marked point. The green region is not in the local network simulation.

4   Simulations

In this section, we present simulation results for three different model problems. The purpose is of these running these examples is to showcase a proof of concept of the proposed multiscale algorithm and its applications to what conventional method cannot compute. We first compare the results computed from full network simulations and the proposed multiscale simulations the a steady state single-phase flow with a nonlinear network flux. This example is designed to demonstrate the convergence of our multiscale coupling algorithm for nonlinear pressure equation. In the second experiment, we presented a very particular setting which is not uncommon in porous media containing either bore holes or fractures that are cemented naturally except at the tips. In such settings, the underlying network contain a highly conducting throat that connects only two widely separated physical locations. In the third example, represent our result of multiphase simulation using the proposed multiscale front tracking algorithm. We note that with the dynamic network model, it is virtually impossible to perform direct simulation over the macroscopic spatial and temporal domains used in the last example.

Experiment 1. (**Quadratic flux for high velocity flows**) The flux f_{ij} in the network model is given by

$$\frac{f_{ij}}{c_{ij}} + \beta f_{ij}^2 = -(p_i - p_j).$$

The formula is derived from the Forchheimer equation:

$$-\frac{\mathrm{d}p}{\mathrm{d}x} = \frac{\mu}{\mathbf{K}} \cdot v + \rho \beta v^2,$$

where p is the pressure, v is the flux velocity, $\mathbf{K}$ is the permeability and μ is the viscosity, ρ is the fluid density and β is the non-Darcy coefficient of the porous medium.

16

The Forchheimer equation is the standard equation for describing high-velocity flow in petroleum engineering [25, 33]. In our simulation, by solving the quadratic equation, we used the following formula:

$$f_{ij} = \frac{-1 + \sqrt{1 - 4\beta c_{ij}^2 (p_i - p_j)}}{2\beta c_{ij}} \simeq - \left(c_{ij} + \beta c_{ij}^3 |p_i - p_j| \right) (p_i - p_j)$$

The conductance in this case is $\left(c_{ij} + \beta c_{ij}^2 |p_i - p_j| \right)$ and depends on nearby pressures p_i and p_j. The parameter β is chosen to be 10^{12} on purpose in order to amplify nonlinear effects in our simulations.

The testing full network model has 1001×21 nodes arranged in a $[0, 1] \times [0, 0.02]$ rectangle domain. Each node is connected by 6 nearby nodes and the length of throats are 0.001 unit in horizontal and vertical direction, and are $\sqrt{2}/1000$ unit in diagonal direction. The radii of the throats are randomly generated from the uniform distribution $[(1 - \lambda)r_0, (1 + \lambda)r_0]$ and the conductance c is determined by

$$c_{ij} = \frac{\pi r^4}{8 \, l\mu}.$$

We choose $r_0 = 0.01$, $\lambda = 0.5$, and $\mu = 1$. The resulting conductances range from 10^{-18} to 10^{-7}. We apply Dirichlet boundary condition in x direction: $p = 100$ on the left hand side and $p = 0$ on the right hand side, and periodic boundary condition in y direction. In the simulations using the proposed mulitscale algorithms, we divide the domain into N blocks, each of the dimension $\delta \times 0.02$, so that the center of each block corresponds to the node $x_{\delta + \frac{l}{2}}$ described in Section 2.3. At the microscopic level, we experimented with a few local networks with different sizes.

We fix $\delta = 0.01, 0.015, 0.02$ and set $N = 5, 10, 20, 30$ to test the convergence of the proposed algorithm. We compare the flux F_D and the pressure P_D computed from direct full simulation on 1001×21 nodes with the flux F_H and the pressure P_H computed by the proposed multiscale algorithm using either sampling methods. The pressure P_D is the average value of fine scale pressure on each y-direction section. The relative errors of flux e_F and of pressure e_P are defined by

$$e_F = \frac{|F_H - F_D|}{|F_D|} \quad \text{and} \quad e_P = \frac{\|P_H - P_D\|_\infty}{\|P_D\|_\infty},$$

where $\| \cdot \|_\infty$ is the supreme norm of vectors.

The average error from 1000 realizations is given below

	e_p			e_f		
	$\delta = 10$	$\delta = 15$	$\delta = 20$	$\delta = 10$	$\delta = 15$	$\delta = 20$
$N = 5$	0.0173	0.0139	0.0114	0.0366	0.0240	0.0193
$N = 10$	0.0127	0.0102	0.0084	0.0322	0.0213	0.0169
$N = 20$	0.0094	0.0071	0.0058	0.0297	0.0193	0.0141
$N = 30$	0.0074	0.0054	0.0041	0.0305	0.0201	0.0150

Experiment 2. (Nonlocal connections in network model. See Figure 6 for a realistic example.) We first set up a regular network as in Experiment 1, except that here we use the linear flux $f_{ij} = -c_{ij}(p_i - p_j)$. The boundary condition is $p = 10$ on both left hand side and $p = 0$ on the right sides and periodic in y direction.

We then create a nonlocal throat connecting pore A at $(0.1, 0.01)$ and pore B at $(0.9, 0.01)$ with conductance c_{nl}. When c_{nl} is relatively larger than other conductances in the network, the pressure values of pore A and pore B are close even their physical positions are far away. The standard coupling method discussed earlier can not capture such behavior. However, the method is modified as following.

In addition to the original macroscopic pressure P_i, we introduce two pressures Q_1 and Q_2 on macro-scale in order to approximate micro pressure of pores A and B. We divide the network into N coarse blocks. Suppose pore A is in the first block and pore B is in the last block. The flux in the nonlocal throat is denoted by $G_0 = -(Q_2 - Q_1)c_{nl}$ and the fluxes on the left boundary and right boundary of the first block is denoted by F_0 and $F_{\frac{1}{2}}$ respectively. Then F_0 and $F_{\frac{1}{2}}$ are functions of P_0, P_1 and Q_1, and we have $F_0 = G_0 + F_{\frac{1}{2}}$. Similarly, we denote $F_{N-\frac{1}{2}}$ and F_N for fluxes on the left boundary and right boundary of the last block. They are functions of P_{N-1}, P_N and Q_2, and we have $F_0 = G_0 + F_{\frac{1}{2}}$. Flux $F_{l-\frac{1}{2}}$ in other blocks is defined as the same as before. Then we look for the macroscopic pressure P_l and Q_1, Q_2 to satisfies mass conservation of flux: $F_0 = G_0 + F_{\frac{1}{2}}$, $F_{l-\frac{1}{2}} = F_{l+\frac{1}{2}}$ for $l = 1, ..., N-1$ and $F_{N-\frac{1}{2}} + G_0 = F_N$. See Figure 7 for illustration.

In the simulations, $c_{nl} = 10^{-5}$ and $N = 5$ coarse blocks are used. The sampling size δ is chosen to be $0.04, 0.08, 0.12, 0.16, 0.2$. The error of pressure and flux is given below:

	$\delta = 0.04$	$\delta = 0.08$	$\delta = 0.12$	$\delta = 0.16$	$\delta = 0.2$
e_p	0.0937	0.0508	0.0228	0.0110	0.000014
e_f	0.2463	0.1180	0.0608	0.0138	0.000006

We observe that the pressure error is reasonably small for all choices of δ. The flux error is large when sampling size is not wide enough, but the error decays when enlarging the sampling size. If we sample all pores in the network ($\delta = 0.2$), we obtain very accurate approximation for pressure and flux of full network simulation. This example demonstrates that our method can be applied to an unstructured network which is very different from discretizations of partial differential equations.

Experiment 3. (Two dimensional problem with two-phase flow)

In the following simulation, we consider a two-dimensional network with 1001×1001 pores whose physical domain is $[-250, 250]^2$. The network structure is regular lattice and each pore connects to four adjacent pores. The spacing between layers of the network in x- and y- directions is 0.5.

While this is a two-dimensional problem, we nevertheless assume 3D shapes for pores and throats so that wetting layers can be accommodated. Pore bodies are cubic shape and throats have square cross-sections.
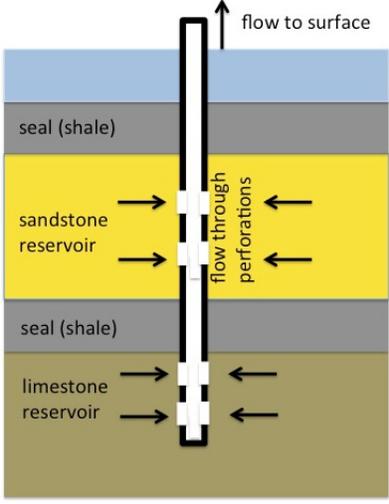
Figure 6: Schematic of a wellbore drilled for exploration of hydrocarbons. The oil flows from the reservoirs through perforations on the wellbore casing: the perforations are the only connection to the neighboring porous formation.
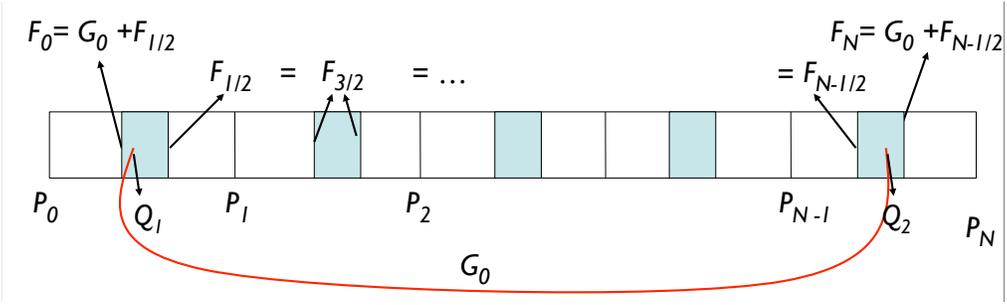
Figure 7: Discretization of the network model with a nonlocal throat. P_i and Q_1, Q_2 denote the macroscopic pressure and F_0, F_N, $F_{i+\frac{1}{2}}$, G_0 denote the macro flux.

19

The radius of inscribed sphere in pore body i is denoted by R_i, and R_i's are generated from a truncated log-normal distribution with no spatial correlation. The density function of R_i takes nonzero value only when $R_{min} \leq R_i \leq R_{max}$ and is given by

$$f(R_i) = c \exp \left[-\frac{1}{2} \left(\frac{\ln(R_i/R_m)}{\sigma_{nd}} \right)^2 \right], \ R_{min} \leq R_i \leq R_{max},$$

where R_{min} is the lower range of truncation, R_{max} is the upper range of truncation, R_m is the mean of inscribed sphere radii, and σ_{nd} is the standard deviation. The constant c is chosen such that $\int_{R_{min}}^{R_{max}} f(R) \, dR = 1$. The inscribed radius r_{ij} and length l_{ij} of the throat ij are then determined based on the values of R_i and R_j as described in [27]. We create a heterogeneity (region with smaller radii of pores and throats), in our domain as follows. We set $R_m = 0.1$, $R_{min} = 0.05$, $R_{max} = 0.25$ and $\sigma_{nd} = 0.1$ in the region $x < y^2/10 + 25$, and $R_m = 0.02$, $R_{min} = 0.01$, $R_{max} = 0.05$ and $\sigma_{nd} = 0.1$ in the region $x > y^2/10 + 25$. The resulting pore radii as well as throat radii are smaller inside the parabolic region $\Omega = \{(x,y) | x > y^2/10 + 25\}$ than ones outside the region Ω.

Initially the network is filled wetting fluid. At time t=0 and onwards, the network is assumed connected to a non-wetting fluid reservoir on the left hand side and a wetting fluid reservoir on the right hand side. Let P_g denote the non-wetting fluid reservoir pressure. Throughout the simulation on the left hand side, the boundary condition is then $p_i^n = P_g$, $p_i^w = 0$ and $s^w = 0$, on the right hand side boundary we have $p_i^n = p_i^w = 0$, and $s^w = 1$. Periodic boundary conditions are imposed at the rest of boundaries.

From the specific shape of pore bodies and throats assumed, the local capillary pressure p_i^c can be computed from the wetting phase saturation s_i^w using the function

$$p_i^c(s_i^w) = \frac{2\sigma^{nw}}{R_i(1 - \exp(-6.83s_i^w))}, \tag{35}$$

where σ^{nw} is interfacial tension, and the entry capillary pressure is defined by

$$\alpha_{ij} = \frac{\sigma^{nw}}{r_{ij}} \left(\frac{1 - \pi/4}{1 - \sqrt{\pi/4}} \right).$$

Physically, the capillary pressure p_i^c cannot be larger than the capillary pressure applied on the RHS boundary (P_g). From the $p_i^c - s_i^w$ relationship (35), we then impose the minimum saturation $s_{i,min}^w$ as follows:

$$s_{i,min}^w = -\frac{1}{6.83} \ln \left(1 - \frac{2\sigma^{nw}}{R_i P_g}, \right). \tag{36}$$

The parameters we use in this numerical experiment are $P_g = 30$, $\sigma = 0.0725$, $\mu_n = \mu_w = 0.001$.

With our current implementation (in MATLAB/Octave), we cannot perform a complete, direct simulation in the entire network in reasonable time. We thus present

a multiscale result using the method described in Section 3.3.1 and 3.3.2. We discretize the domain $[-250, 250]^2$ into 20×20 coarse blocks and use a fixed time step size Δt equal to 3. We refer to the grid lines by x_i and y_j. The boundary conditions for macroscopic pressure P are consistent with the network model: $P = P_g = 30$ in the left side and $P = 0$ in the right hand side, and periodic in the rest of boundary.

The evolution of the front $\Gamma(t)$ is assumed to be well described as a function of y. The initial front $\Gamma(t)$ is simply the grid line $x = -250$ and the evolution of $\Gamma(t)$ is tracked by the marked points $(x_j(t), y_j)$. At each time t_n, we solve for the pressure field P_{ij} at the grid node (x_i, y_j). The marked points is then moved according to the local two-phase network simulations. We choose the local network size to be 10×10 and the local simulation time δt to be 1.5. See the left figure in Figure 9 for an illustration. We use cubic spline interpolation on updated marked point to obtain full $\Gamma(t)$ at t_{n+1}, and reassign marked points as $(x_j(t_{n+1}), y_j)$, i.e. the intersection of $\Gamma(t_{n+1})$ and grid line y_j. The total simulation time is 180. In Figure 8, we show snapshots of saturation at three different times. We observe that the front $\Gamma(t)$ is roughly a straight line before it reaches the area $x > y^2/10 + 25$. When it reaches the region Ω, the front can not move into the area because the speed of the marked points on the intersection of $\Gamma(t)$ and the boundary of Ω is very small (due to the parabolic region with smaller pores/throats). See the left figure in Figure 8. The capillary pressure of each pore at $t = 126$ is shown in the right figure in Figure 8. By the definition of minimum saturation and our downscaling method, the capillary pressure of the pores behind the front is $P_g = 30$. Because the throats' radii is smaller in Ω, its capillary force is larger than other pores ahead the front. When the entry capillary pressure α_{ij} is lager than P_g, the non-wetting fluid can never invade the pores.

This phenomenon cannot be easily captured by continuous approaches that neglect capillary pressure. Furthermore, the approach we present can be conceptually extended to cases where the pore scale simulation parameters dynamically responded to changes in macroscopic parameters (see fracture example in [14]).

5   Conclusion

The algorithms presented in this article are built upon the HMM method introduced in [14], where single-phase flow is considered. We presented some careful numerical convergence studies for the proposed method. The existing single-phase algorithms is here extended to handle the special scenarios where nonlocal edges in the network develops during the drilling. Conventional PDE based method cannot easily model such type of problems. The new mulitscale two-phase front tracking algorithm is able to advance the front using a dynamic two-phase network model. There is no difficulty in building a level set method that allows for different portions of the front to merge or break up. The purpose of the present paper is to serve as a proof of concept in evaluation of macroscopic front speed using more accurate two-phase network models.
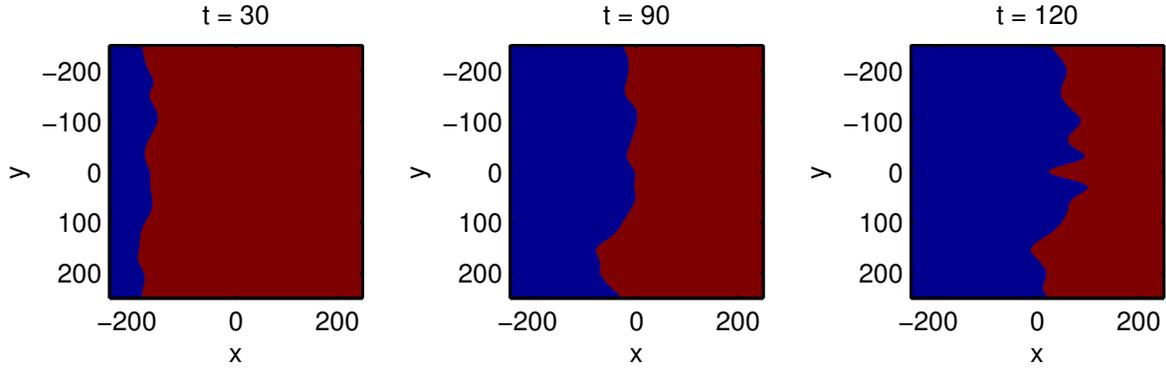
Figure 8: Snapshot of saturation at $t = 30, 90, 120$. The blue region is where pore bodies are filled with non-wetting phase fluid ($s_i^w = s_{i,min} \sim 0$). The red region is where pore bodies are not invaded ($s_i^w = 1$).
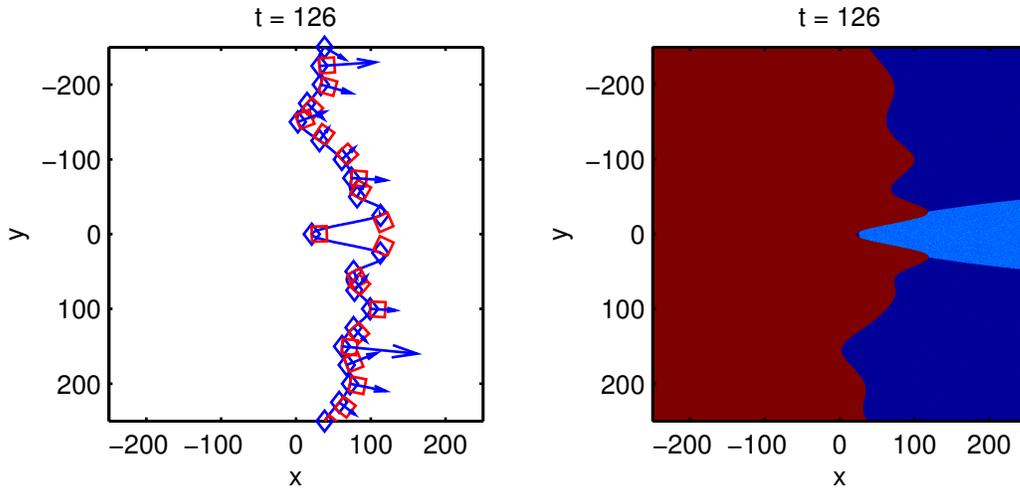
Figure 9: Left Figure: Illustrations of front curve with sampling domains when $t = 126$. The blue arrows indicate the direction of velocity of marked point obtained from local network simulation. Right Figure: Capillary pressure p^c at the pores when $t = 126$. The value in the red region is 30, the value in the light blue is in between 7 and 8, and the value in the dark blue region is in between 1 and 2.

6 Acknowledgements

References

[1] T. Arbogast. Gravitational forces in dual-porosity systems: 1. model derivation by homogenization. *Transport in Porous Media*, 13(2):179–203, 1993.

[2] T. Arbogast. Gravitational forces in dual-porosity systems: 2. computational validation of the homogenized model. *Transport in Porous Media*, 13(2):205–220, 1993.

[3] T. Arbogast, L.C. Cowsar, M.F. Wheeler, and I. Yotov. Mixed finite element methods on nonmatching multiblock grids. *SIAM J. Numer. Anal.*, 37(4):1295–1315, APR 27 2000.

[4] M. T. Balhoff, K. E. Thompson, and M Hjortso. Coupling pore-scale networks to continuum-scale models of porous media. *Computers and Geosciences*, 33(3):393–410, 2007.

[5] Matthew Balhoff, Sunil Thomas, and Mary Wheeler. Mortar coupling and upscaling of pore-scale models. *Computational Geosciences*, 12:15–27, 2008. 10.1007/s10596-007-9058-6.

[6] M.J. Blunt. Flow in porous media - pore-network models and multiphase flow. *Current Opinion Colloid Interface Sci.*, 6:197–207, 2001.

[7] M.J. Blunt, M.D. Jackson, M. Piri, and P.H. Valvatne. Detailed physics, predictive capabilities and macroscopic consequences for pore-network models of multiphase flow. *Adv. Water. Resour.*, 25:1069–1089, 2002.

[8] S.L. Bryant, P.R. King, and D.W. Mellor. Network model evaluation of permeability and spatial correlation in a real random sphere packing. *Transport Porous Media*, 11:53–70, 1993.

[9] M.A. Celia, P.C. Reeves, and L.A. Ferrand. Recent advances in pore-scale models for multiphase flow in porous media. *Rev. Geophys. Suppl.*, 33:1049–1057, 1995.

[10] Y. Chen and L. J. Durlofsky. An adaptive local-global upscaling for general flow scenarios in heterogeneous formations. *Transport in Porous Media*, 62:157–185, 2006.

[11] Y. Chen and L.J. Durlofsky. Efficient incorporation of global effects in upscaled models of two-phase flow and transport in heterogeneous formations. *SIAM MMS*, 5:445–475, 2006.

[12] Y. Chen, L.J. Durlofsky, M. Gerritsen, and X.H. Wen. A coupled local-global upscaling approach for simulating flow in highly heterogeneous formations. *Adv. Wat. Res.*, 26:1041–1060, 2003.

[13] Zhangxin Chen, Guanren Huan, and Yuanle Ma. *Computational methods for multiphase flows in porous media*. Computational Science & Engineering. Society for Industrial and Applied Mathematics (SIAM), Philadelphia, PA, 2006.

[14] J. Chu, B. Engquist, M. Prodanović, and R. Tsai. A multiscale method coupling network and continuum models in porous media I – steady state single phase flow. *Under review.*, 2011.

[15] A.B. Dixit, J.S. Buckley, S.R. McDougall, and K.S. Sorbie. Empirical measures of wettability in porous media and the relationship between them derived from pore-scale modelling. *Transport Porous Media*, 40:27–54, 2000.

[16] L. J. Durlofsky, Y. Efendiev, and V. Ginting. An adaptive local-global multiscale finite volume element method for two-phase flow simulations. *Adv. Wat. Res.*, 30:576–588, 2007.

[17] W. E and B. Engquist. The heterogeneous multi-scale methods. *Comm. Math. Sci*, 1(1):87–133, 2003.

[18] Y. Efendiev, V. Ginting, T. Y. Hou, and R. Ewing. Accurate multiscale finite element methods for two-phase flow simulations. *J. Comput. Phys.*, 220(1):155–174, 2006.

[19] Y. Efendiev and T. Y. Hou. *Multiscale finite element methods: Theory and applications*. Springer, New York, 2009.

[20] Bjorn Engquist, Russel Caflisch, and Yi Sun. A multiscale method for epitaxial growth. *Multiscale Model. Simul.*, 9(1):335–354, 2011.

[21] Bjorn Engquist and Yi Sun. Heterogeneous multiscale methods for interface tracking of combustion fronts. *Multiscale Model. Simul.*, 5(2):532–563, 2006.

[22] I. Fatt. The network model of porous media I. Capillary characreristics. *Pet. Trans. AIME*, 207:144–159, 1956a.

[23] I. Fatt. The network model of porous media II. Dynamic properties of a single size tube network. *Pet. Trans. AIME*, 207:160–163, 1956b.

[24] I. Fatt. The network model of porous media III. Dynamic properties of networks with tube radius distribution. *Pet. Trans. AIME*, 207:164–181, 1956c.

[25] P. Forchheimer. *Hydrolik*. Teubner, Leipzig and Berlin, 1914.

[26] M. Hilpert and C.T. Miller. Pore-morphology-based simulation of drainage in totally wetting porous media. *Adv. Water. Resour.*, 24:243–255, 2001.

[27] V. Joekar-Niasar, S. M. Hassanizadeh, and H. K Dahle. Non-equilibrium effects in capillarity and interfacial area in two-phase flow: dynamic pore-network modelling. *J. Fluid Mech.*, 655:38–71, 2010.

[28] M. Karimi-Fard, B. Gong, and L. J. Durlofsky. Generation of coarse-scale continuum flow models from detailed fracture characterization. *Water Res. Research*, 42(10), 2007.

[29] Jon E. Olson, Stephen E. Laubach, and Robert H. Lander. Natural fracture characterization in tight gas sandstones: Integrating mechanics and diagenesis. *AAPG Bulletin*, 93(11):1535–1549, November 2009.

[30] P.E. Oren and S. Bakke. Reconstruction of Berea sandstone and pore-scale modelling of wettability effects. *J. Petroleum Sci. Eng.*, 39:177–199, 2003.

[31] P.C. Reeves and M.A. Celia. A functional relationship between capillary pressure, saturation, and interfacial area as revealed by a pore scale network model. *Water Resour. Res.*, 32:2345–2358, 1996.

[32] F. D. Rossa, C. D'Angelo, and A. Quarteroni. A distributed model of traffic flows on extended regions. *Networks and Heterogeneous Media*, 5(3), 2010.

[33] F. Thauvin and K. K. Mohanty. Network modeling of non-darcy flow through porous media. *Transport in Porous Media*, 31:19–37, 1998.

[34] K. E. Thompson. Pore-scale modelling of fluid transport in disordered fibrous materials. *AIChE J.*, 48:11369–1389, 2002.

[35] P.H. Valvatne and M.J. Blunt. Predictive pore-scale modeling of two-phase flow in mixed wet media. *Water Resour. Res.*, 40:W07406, 2004.

[36] M.I.J. van Dijke, K.S. Sorbie, and S.R. McDougall. Saturation-dependencies of three-phase relative permeabilities in mixed-wet and fractionally wet systems. *Adv. Water. Resour.*, 24:365–384, 2001.

[37] X. Wang and K.K. Mohanty. Pore-network model of flow in gas-condensate reservoirs. *SPE J.*, 5:426–34, 2000.

[38] Stephen Whitaker. Flow in porous media i: A theoretical derivation of darcy's law. *Transport in Porous Media*, 1:3–25, 1986.

[39] S. Youssef, M. Han, D. Bauer, E. Rosenberg, S. Bekri, M. Fleury, and O. Vizika. High resolution μCT combined to numerical models to assess electrical properties of bimodal carbonates. Abu Dhabi, UAE, 29 October - 2 November 2008.

[40] D. Zhou, M. J. Blunt, and F. M. Orr. Hydrocarbon drainage along corners of noncircular capillaries. *J. Colloid Interface Sci.*, 187:11–21, 1997.